

# Element Free Galerkin Method for Three-dimensional Structural Analysis

Wen-Hwa Chen<sup>1</sup> and Xhu-Ming Guo<sup>2</sup>

**Abstract:** An Element Free Galerkin Method is developed for the analysis of three-dimensional structures. A highly accurate and reliable relation between the number of the quadrature orders  $n_Q$  and nodes in a three-dimensional cell  $n_c$ ,  $n_Q \geq \sqrt[3]{n_c} + 3$ , is established to accomplish the required integral calculation in the cell. Based on the theory of topology, the generation of nodes in the solution procedure consists of three sequential steps, say, defining the geometric boundary, arranging inside of the body, and improving numerical accuracy. In addition, by selecting the Dirac Delta function as the weighting function, a three-dimensional scattering sub-domain is devised by linking the node studied to neighbor nodes. Since the size of this newly defined sub-domain is adjustable with the nodal density, the three-dimensional scattering sub-domain can execute the moving least square approximation resiliently, but excellent accuracy is still maintained. Several numerical examples have been studied successfully to demonstrate the proposed techniques.

## 1 Introduction

In most of actual engineering problems, the analytical solutions are hardly derivable and even nonexistent because of their complicated geometry conditions. In dealing with such problems, finite element method has demonstrated its high versatility and efficiency. However, the accuracy of the finite element method sometimes has its own limitations, especially in solving the problems with curved boundaries or specific complicated surfaces. To improve the results, a very detailed finite element mesh is usually required.

Recently, the Element Free Galerkin Method (EFGM, Belytschko et al., 1994) has become an interesting and

promising method in solving partial differential equations or structural mechanics problems due to its vast flexibility in practical applications. Unlike finite element method, EFGM requires only nodal data and the nodal interpolation functions are derived by the moving least squares approximation. However, to generate the "stiffness matrix" or the evaluation of the "energy", the EFGM method still uses background cells. A new class of truly meshless methods, one based on the local symmetric weak-form called the Meshless Local Petrov-Galerkin (MLPG) Method, and the other based on the Local Boundary Integral Equation (LBIE), have been recently proposed by Atluri and his research collaborators (Atluri et al., 1998a,b,c; 1999; 2000a,b,c,d; 2001) (See also Chung and Batra (2001)).

Starting from the original idea of Nayroles et al. (1992), Belytschko et al. (1994; 1996a) popularized the EFGM to the analysis of various structural mechanics problems. Those include the stress analysis of cantilever beam, plate and shell. Several approaches were further studied for enforcing the essential boundary conditions by Lagrange multiplier method (Belytschko et al., 1994; 1995), modified collocation and penalty method (Zhu et al., 1998) and the combined FEM-EFGM method (Belytschko et al., 1995; 1996b; Hegen, 1996; Mukherjee et al., 1997). In addition, the continuity of nodal interpolation functions adopted and convergence of EFGM solutions were also analyzed. (Belytschko et al., 1996c; 1997).

In those literatures as mentioned above, all the investigations were limited to one or two-dimensional problems, or simplified as plate and shell structures. However, in practical engineering applications, a three-dimensional analysis is imperative for most structures. Besides, a circle sub-domain for two-dimensional problems is adopted in those literatures for executing the moving least squares approximation. (However, in Atluri et al. (1999), elliptical and rectangular subdomains were used, for the first time, in generating the moving least squares approxima-

---

<sup>1</sup> Professor, corresponding author  
Department of Power Mechanical Engineering  
National Tsing Hua University  
Hsinchu, Taiwan 30043, Republic of China  
E-mail : whchen@pme.nthu.edu.tw

<sup>2</sup> Graduate student

tions, as well as in enforcing the local Petrov-Galerkin weak form.) In general, the radius of the circle sub-domain is a pre-decided parameter and will affect the bandwidth of stiffness matrix and, therefore the computational efficiency seriously. This is mainly induced from including unnecessary nodes in some circle sub-domains with higher density of neighbor nodes. The deficiency will be enlarged in three-dimensional analysis. To improve this, a new computational scheme which can be used for dealing with three-dimensional cells and nodal generations needs to be developed.

One of the objectives of this work is to extend the EFGM to the analysis of three-dimensional structural problems. To remove the size and shape constraints of the circle sub-domain used in literatures, a three-dimensional scattering sub-domain is devised in this work. In addition, a new integration relation for defining the numbers of the quadrature orders  $n_Q$  and nodes existing in the three-dimensional cell  $n_c$  is established as  $n_Q = \sqrt[3]{n_c} + 3$ . Based on the theory of topology, the nodal set  $\mathbf{X}$  consists of three subsets, say, boundary description  $\mathbf{X}_{boundary}$ , body arrangement  $\mathbf{X}_{body}$ , and numerical improvement  $\mathbf{X}_{improvement}$ . That is,  $\mathbf{X} = \mathbf{X}_{boundary} + \mathbf{X}_{body} + \mathbf{X}_{improvement}$ . To demonstrate the applicability and versatility of the present techniques developed, three numerical examples are analyzed. For the comparison of computational efficiency between EFGM and finite element method, a three-dimensional stress concentration analysis around a circular cylinder subjected to uniform loading at both ends is first performed. A sphere under a diametrical loading at two poles is then analyzed to display the flexibility of EFGM presented. The last example, which simulates the forward motion of a screwdriver, is focused on the demonstration of the novelty of the three-dimensional scattering sub-domain in executing moving least squares approximation even among nodes with different densities. These should be of help for EFGM in three-dimensional structural problems.

## 2 Formulation of EFGM

As shown in Fig.1 consider a three-dimensional linear elastic structure  $\Omega$ , enclosed by the boundary  $\Gamma$ . As the system is in static equilibrium condition, the governing equation can be written as follows:

$$\nabla \cdot \sigma + \mathbf{b} = 0 \text{ in } \Omega,$$

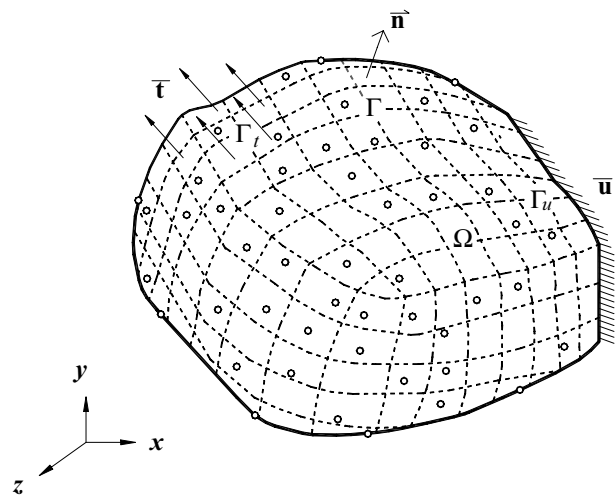


**Figure 1** : Three-dimensional structural analysis by EFGM

where  $\sigma$  is the stress tensor and  $\mathbf{b}$  is the body force vector. The corresponding boundary conditions are

$$\sigma \cdot \mathbf{n} = \bar{\mathbf{t}} \text{ on } \Gamma_t,$$

and

$$\mathbf{u} = \bar{\mathbf{u}} \text{ on } \Gamma_u,$$

in which  $\bar{\mathbf{t}}$  is the prescribed traction vector acting on the traction boundary  $\Gamma_t$ ,  $\bar{\mathbf{u}}$  is the prescribed displacement on the displacement boundary  $\Gamma_u$ , and  $\mathbf{n}$  is the outward unit normal to the boundary  $\Gamma$ .

Based on the principle of minimum total potential energy (Cook et al., 1989),

$$\Pi = U - W = \min, \tag{1}$$

in which  $U$  is the strain energy of the system, and  $W$  is the work done by external loads. Assume the structure has no initial stress or initial strain, then

$$U = \frac{1}{2} \int_{\Omega} \sigma \epsilon d\Omega = \frac{1}{2} \int_{\Omega} \epsilon^T E \epsilon d\Omega \tag{2}$$

and

$$W = \int_{\Omega} \mathbf{u}^T \mathbf{b} d\Omega + \int_{\Gamma_t} \mathbf{u}^T \bar{\mathbf{t}} d\Gamma, \tag{3}$$

where  $\mathbf{E}$  is the material property matrix and  $\boldsymbol{\varepsilon}$  is the strain tensor. Substituting Eqns(2) and (3) into Eqn.(1), Eqn.(1) becomes

$$\Pi = \frac{1}{2} \int_{\Omega} \boldsymbol{\varepsilon}^T \mathbf{E} \boldsymbol{\varepsilon} d\Omega - \int_{\Omega} \mathbf{u}^T \mathbf{b} d\Omega - \int_{\Gamma_t} \mathbf{u}^T \bar{\mathbf{t}} d\Gamma = \min \quad (4)$$

Following the similar formulation procedure for one or two-dimensional structural problems (Belytschko et al., 1994 etc.)<sup>3</sup>, the present three-dimensional displacement field  $\mathbf{u}$  can be expressed as a function of nodal displacements such that

$$\mathbf{u}^T = \{ u(\mathbf{x}) \quad v(\mathbf{x}) \quad w(\mathbf{x}) \}, \quad (5)$$

where

$$u(\mathbf{x}) = \sum_{i=1}^N \phi_i(\mathbf{x}) \hat{u}_i,$$

$$v(\mathbf{x}) = \sum_{i=1}^N \phi_i(\mathbf{x}) \hat{v}_i,$$

and

$$w(\mathbf{x}) = \sum_{i=1}^N \phi_i(\mathbf{x}) \hat{w}_i.$$

In the above expressions,  $\{u(\mathbf{x}) \quad v(\mathbf{x}) \quad w(\mathbf{x})\}$  denote the displacement components at location  $\mathbf{x}$  in  $x$ ,  $y$  and  $z$  directions, respectively.  $\{\hat{u}_i \quad \hat{v}_i \quad \hat{w}_i\}$  are the nodal displacement components in three different directions of node  $i$  and  $N$  is the total amount of nodes taken in the analysis model.  $\phi_i(\mathbf{x})$  is the nodal interpolation function of node  $i$ , which is derived by a moving least squares approximation and will be discussed in the next section. Now, the three-dimensional displacement field  $\mathbf{u}$  of Eqn.(5) can be rewritten in the global form as

$$\mathbf{u} = \boldsymbol{\Psi}(\mathbf{x}) \mathbf{D}, \quad (6)$$

where

$$\boldsymbol{\Psi}(\mathbf{x}) = \begin{bmatrix} \phi_1(\mathbf{x}) & 0 & 0 & \phi_2(\mathbf{x}) & 0 & 0 & \cdots & \phi_N(\mathbf{x}) & 0 & 0 \\ 0 & \phi_1(\mathbf{x}) & 0 & 0 & \phi_2(\mathbf{x}) & 0 & \cdots & 0 & \phi_N(\mathbf{x}) & 0 \\ 0 & 0 & \phi_1(\mathbf{x}) & 0 & 0 & \phi_2(\mathbf{x}) & \cdots & 0 & 0 & \phi_N(\mathbf{x}) \end{bmatrix}_{3 \times 3N}$$

<sup>3</sup>It should be remarked that while the EFGM uses the global weak form  $\delta\Pi = 0$  from Eqn.(4), the MLPG and LBIE methods pioneered by Atluri and his collaborators (1998 a,b,c; 1999; 2000a,b,c,d; 2001) use a local weak form over non-overlapping subdomains, and thus generate a truly meshless method.

and

$$\mathbf{D}^T = \{ \hat{u}_1 \quad \hat{v}_1 \quad \hat{w}_1 \quad \hat{u}_2 \quad \hat{v}_2 \quad \hat{w}_2 \quad \cdots \quad \hat{u}_N \quad \hat{v}_N \quad \hat{w}_N \}_{1 \times 3N}$$

By the strain-displacement relation, one has

$$\boldsymbol{\varepsilon} = \partial \mathbf{u} = \partial \boldsymbol{\Psi}(\mathbf{x}) \mathbf{D} = \mathbf{B}(\mathbf{x}) \mathbf{D}, \quad (7)$$

where the partial differential operator  $\partial$  and the strain-displacement matrix  $\mathbf{B}(\mathbf{x})$  are defined as

$$\partial = \begin{bmatrix} \partial/\partial x & 0 & 0 \\ 0 & \partial/\partial y & 0 \\ 0 & 0 & \partial/\partial z \\ \partial/\partial y & \partial/\partial x & 0 \\ 0 & \partial/\partial z & \partial/\partial y \\ \partial/\partial z & 0 & \partial/\partial x \end{bmatrix}_{6 \times 3}$$

and

$$\mathbf{B}(\mathbf{x}) = \begin{bmatrix} \phi_{1,x}(\mathbf{x}) & 0 & 0 & \cdots & \phi_{N,x}(\mathbf{x}) & 0 & 0 \\ 0 & \phi_{1,y}(\mathbf{x}) & 0 & \cdots & 0 & \phi_{N,y}(\mathbf{x}) & 0 \\ 0 & 0 & \phi_{1,z}(\mathbf{x}) & \cdots & 0 & 0 & \phi_{N,z}(\mathbf{x}) \\ \phi_{1,y}(\mathbf{x}) & \phi_{1,x}(\mathbf{x}) & 0 & \cdots & \phi_{N,y}(\mathbf{x}) & \phi_{N,x}(\mathbf{x}) & 0 \\ 0 & \phi_{1,z}(\mathbf{x}) & \phi_{1,y}(\mathbf{x}) & \cdots & 0 & \phi_{N,z}(\mathbf{x}) & \phi_{N,y}(\mathbf{x}) \\ \phi_{1,z}(\mathbf{x}) & 0 & \phi_{1,x}(\mathbf{x}) & \cdots & \phi_{N,z}(\mathbf{x}) & 0 & \phi_{N,x}(\mathbf{x}) \end{bmatrix}_{6 \times 3N}$$

The weak form of Eqn. (4) leads to the following total potential energy in matrix form as

$$\Pi = \frac{1}{2} \mathbf{D}^T \mathbf{K} \mathbf{D} - \mathbf{D}^T \mathbf{R}, \quad (8)$$

where the stiffness matrix  $\mathbf{K}$  and load vector  $\mathbf{R}$  are shown as  $\mathbf{K} = \int_{\Omega} \mathbf{B}(\mathbf{x})^T \mathbf{E} \mathbf{B}(\mathbf{x}) d\Omega$ ,

and

$$\mathbf{R} = \int_{\Omega} \boldsymbol{\Psi}(\mathbf{x})^T \mathbf{b} d\Omega + \int_{\Gamma_t} \boldsymbol{\Psi}(\mathbf{x})^T \bar{\mathbf{t}} d\Gamma.$$

Among all admissible configurations of the present conservative system, since the strain energy density is positive definite, those that satisfy the system of equilibrium will make the total potential energy minimum. Thus, from the stationary condition of Eqn.(8) one obtains

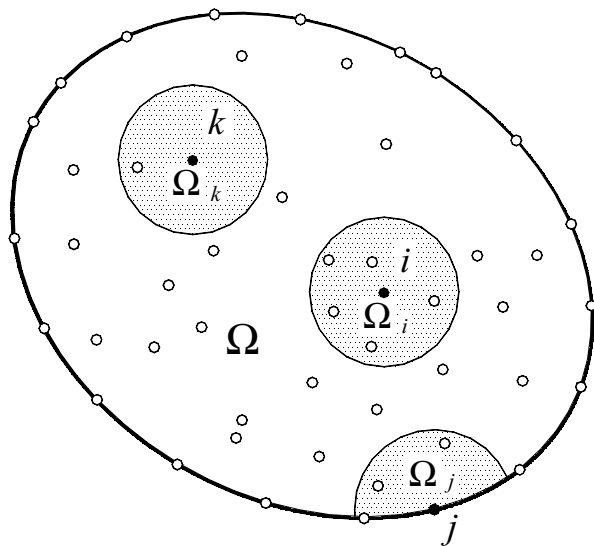


Figure 2 : The circle sub-domain

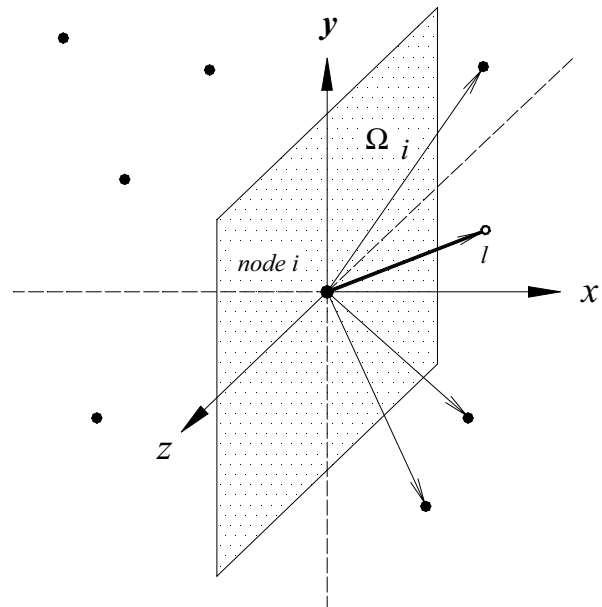


Figure 3 : The three-dimensional scattering sub-domain

$$KD = R \tag{9}$$

By solving the system of linear algebraic equations of Eqn.(9), the global nodal displacement vector  $\mathbf{D}$  is determined. Finally, all the unknowns  $\mathbf{u}$  and  $\epsilon$ , and therefore  $\sigma$ , can then be computed from Eqn.(6) and Eqn.(7), respectively.

### 3 Three-dimensional Scattering Sub-domain

To construct the nodal interpolation function  $\phi_i(x)$  of node  $i$ , a circle sub-domain around node  $i$  is usually adopted to choose the neighbor nodes within the circle as the domain influential basis (Belytschko et al., 1994). As seen in Fig.2,  $\Omega_i$  and  $\Omega_k$  denote the circle sub-domains of inner nodes  $i$  and  $k$ , while the boundary node  $j$  is surrounded by a portion of circle sub-domain  $\Omega_j$ . Since the radius of circle sub-domains is pre-decided and unchangeable, different amounts of nodes may exist in each sub-domain. Hence, much wider bandwidth will occur in the sub-domains having more neighbor nodes. This will decrease the computational efficiency seriously, especially for three-dimensional structural analysis.

To overcome this deficiency, a simple but efficient three-dimensional scattering sub-domain is devised in this

work. The nodal connections between node  $i$  and its neighbor nodes are displayed in Fig.3. For a specific direction, say  $x > 0$ , the nearest neighbor node  $l$  is selected as the domain influential basis. Therefore, the present three-dimensional scattering sub-domain developed for inner nodes always contains six linkages between node  $i$  and the nearest neighbor node in respective directions ( $\pm x, \pm y, \text{ and } \pm z$  directions). For boundary nodes, the sub-domain may contain one to five neighbor nodes. Apparently, this three-dimensional scattering sub-domain has the following advantages:

- (a) The pre-decided radius of circle sub-domain is not necessary. Since each node has one to six neighbor nodes for three-dimensional structural problems, the bandwidth of stiffness matrix can be accurately predicted and flexibly controlled even when the nodes are distributed in the medium randomly.
- (b) To derive the nodal interpolation functions, simpler weighting function is sufficient.
- (c) The nodes can be added or deleted freely without destroying the entire linkages. The adjustment only changes the moving least squares approximation of corresponding neighbor nodes.

Without loss of generality, the nodal interpolation functions can be derived based on the displacement component in  $x$  direction  $u(x)$ . According to the three-

dimensional scattering sub-domain established,  $u(x)$  in the sub-domain  $\Omega_i$  can be expressed by

$$u(x) = \mathbf{p}^T(x) \mathbf{a}(x), \quad \forall x \in \Omega_i \tag{10}$$

where  $\mathbf{p}^T(x) = \{p_1(x), p_2(x), p_3(x), \dots, p_m(x)\}_{1 \times m}$  is a complete monomial basis of order  $m$ ,  $\mathbf{a}(x)$  is a coefficient vector  $\mathbf{a}^T(x) = \{a_1(x), a_2(x), a_3(x), \dots, a_m(x)\}_{1 \times m}$ .  $\mathbf{x} = \{x \ y \ z\}^T$  is a vector of space coordinates. Hence, for a three-dimensional problem, for example,

$$\begin{aligned} \mathbf{p}^T(x) &= \{1, x, y, z\}_{1 \times m}, \text{ linear basis; } m = 4; \\ \mathbf{p}^T(x) &= \{1, x, y, z, x^2, y^2, z^2, xy, yz, zx\}_{1 \times m}, \text{ quadratic basis; } \\ & m = 10; \\ & \dots \end{aligned}$$

The coefficient vector  $\mathbf{a}(x)$  can be determined by minimizing a weighting discrete  $L_2$  norm, which is defined as (Belytschko et al., 1994)

$$\begin{aligned} J(x) &= \sum_{i=1}^n w_i(x) (\mathbf{p}^T(x_i) \mathbf{a}(x) - \hat{u}_i)^2 \\ &= [\mathbf{P} \mathbf{a}(x) - \hat{\mathbf{u}}]^T \mathbf{W} [\mathbf{P} \mathbf{a}(x) - \hat{\mathbf{u}}], \end{aligned} \tag{11}$$

where  $w_i(x)$  and  $x_i$  are the weighting function and coordinate associated with the node  $i$ ,  $\hat{u}_i$  is the nodal displacement component in  $x$  direction of node  $i$ , and  $n$  is the number of nodes in the sub-domain  $\Omega_i$ . The nodal displacement fields in  $x$  direction of all nodes  $\hat{\mathbf{u}}$  in the sub-domain can be expressed as

$$\hat{\mathbf{u}}^T = [\hat{u}_1, \hat{u}_2, \dots, \hat{u}_n]_{1 \times n}.$$

Matrices  $\mathbf{P}$  and  $\mathbf{W}$  are defined as

$$\mathbf{P} = \begin{bmatrix} \mathbf{p}^T(x_1) \\ \mathbf{p}^T(x_2) \\ \dots \\ \mathbf{p}^T(x_n) \end{bmatrix}_{n \times m},$$

and

$$\mathbf{W} = \begin{bmatrix} w_1(x) & \dots & 0 \\ \dots & \dots & \dots \\ 0 & \dots & w_n(x) \end{bmatrix}_{n \times n}.$$

The stationary condition of weighting discrete norm  $J(x)$  in Eqn.(11) with respect to the coefficient vector  $\mathbf{a}(x)$  leads to the relation

$$\mathbf{A}(x) \mathbf{a}(x) = \mathbf{C}(x) \hat{\mathbf{u}}, \tag{12}$$

where

$$\mathbf{A}(x) = \mathbf{P}^T \mathbf{W} \mathbf{P} = \mathbf{C}(x) \mathbf{P} = \sum_{i=1}^n w_i(x) \mathbf{p}(x_i) \mathbf{p}^T(x_i),$$

and

$$\mathbf{C}(x) = \mathbf{P}^T \hat{\mathbf{W}} = [w_1(x) \mathbf{p}(x_1), w_2(x) \mathbf{p}(x_2), \dots, w_n(x) \mathbf{p}(x_n)]_{m \times n}.$$

$\mathbf{a}(x)$  in Eqn.(12) has unique solution only when the matrix  $\mathbf{A}(x)$  in Eqn.(12) is non-singular, if and only if the rank of matrix  $\mathbf{P}$  equals  $m$ . This can be achieved by choosing appropriate weighting functions. Solving for  $\mathbf{a}(x)$  from Eqn.(12), one obtains

$$\mathbf{a}(x) = \mathbf{A}^{-1}(x) \mathbf{C}(x) \hat{\mathbf{u}}. \tag{13}$$

Substituting Eqn.(13) into Eqn.(10) one obtains

$$u(x) = \Phi(x) \hat{\mathbf{u}}$$

where

$$\Phi(x) = \mathbf{p}^T(x) \mathbf{A}^{-1}(x) \mathbf{C}(x)$$

or

$$\Phi(x) = [\phi_1(x), \phi_2(x), \dots, \phi_n(x)]_{1 \times n}$$

and

$$\phi_i(x) = \sum_{j=1}^m p_j(x) [\mathbf{A}^{-1}(x) \mathbf{C}(x)]_{ji}.$$

The nodal interpolation function  $\phi_i(x)$  of node  $i$  can be thus derived. Unlike the exponential or conical weighting functions used in literatures (Belytschko et al., 1994), due to the three-dimensional scattering sub-domain adopted, the Dirac Delta function seems to be an appropriate choice for weighting function and is thus taken in this work. Much simpler form of interpolation functions  $\phi_i(x)$  and corresponding differential term in  $\mathbf{B}(x)$  of Eqn.(7) is observed.

#### 4 Computational Scheme

To execute EFGM, although one need not calculate the element property like finite element method, the structure

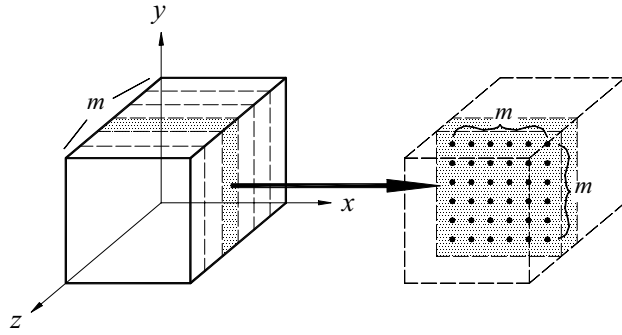


**Figure 4 :** A three-dimensional cell with uniform nodal collocation

need be divided into smaller cells and, similarly, the cell property is integrated by the Gaussian quadrature (Stroud et al., 1996).

For three-dimensional structural problems, for convenience, those cells can be viewed as cuboid. Because the selection of the quadrature orders  $n_Q$  plays an important role on the accuracy of EFGM, the relation between the total number of nodes in a cell  $n_c$  and the quadrature orders  $n_Q$  should be explored. As shown in Fig.4, assume the cell is a perfect one (without void or crack) and the nodes are distributed uniformly. Let  $m$  be defined as the amount of nodes on each line (without counting those two points located at the interface of cell) along single direction of Euclidean coordinates of the cell. The relation between  $n_c$  and  $m$  can be found as (Stroud et al., 1966)

$$m = \sqrt[3]{n_c},$$

where  $D$  is the degrees of dimension for problem. After mapping  $\phi_i(x)$  from global coordinates  $\{x,y,z\}$  to natural coordinates  $\{\xi,\eta,\zeta; -1 \leq \xi,\eta,\zeta \leq 1\}$ , one has

$$\phi_i(x) = \phi_i(\xi, \eta, \zeta) = \sum_{k=1}^K c_k \xi^r \eta^s \zeta^t, \quad (14)$$

where  $r,s$  and  $t$  are the dimensional orders and  $K$  denotes the number of terms used for describing the nodal interpolation functions  $\phi_i(\xi,\eta,\zeta)$  (see Appendix A). For one-dimensional problems,  $s = t = 0$ ; but for two-dimensional problems,  $t = 0$ . It is noted that the nodal interpolation function  $\phi_i(\xi,\eta,\zeta)$  of node  $i$  should be continuous in the cell and at the interfaces of neighboring

cells. Hence, the nodal interpolation functions  $\phi_i(\xi,\eta,\zeta)$  are at least a function of order  $m + 1$  for  $m$  nodes, no matter what kind of weighting function  $w_i(x)$  or influential basis  $p(x)$  is used.

By the implementation of Gaussian quadrature in finite element method (Stroud et al., 1966),

$$r + s + t \geq m + D$$

or

$$r + s + t \geq \sqrt[3]{n_c} + D,$$

That is, the lowest order of the nodal interpolation functions  $\phi_i(\xi,\eta,\zeta)$ ,  $r + s + t$ , is  $\sqrt[3]{n_c} + D$  with respect to the dimensional orders  $r,s$  and  $t$ . According to the definition of Gaussian quadrature (Stroud et al., 1966) and Eqn.(14), the quadrature orders  $n_Q$  can be determined as

$$n_Q \geq O(\phi_i(\xi, \eta, \zeta)) - O(\text{continuity}) + 1,$$

where  $O(\phi_i(\xi, \eta, \zeta))$  is the orders of nodal interpolation functions  $\phi_i(\xi, \eta, \zeta)$ , and  $O(\text{continuity})$  is the physical continuity of the solution. From above discussion, the lowest order  $O(\phi_i(\xi, \eta, \zeta))$  of interpolation functions equals  $\sqrt[3]{n_c} + D$ , and  $O(\text{continuity}) = 1$  for the three-dimensional structural problems tackled. Since the determinant of Jacobian matrix may involve some parameters of  $\xi, \eta, \zeta$  in mapping process, for reserving enough order to get sufficient accuracy, the quadrature order  $n_Q$  is therefore suggested as

$$n_Q \geq \sqrt[3]{n_c} + D \quad (15)$$

For two dimensional problems  $D = 2$ , Eqn.(15) becomes  $n_Q \geq \sqrt{n_c} + 2$ . Once the determinant of Jacobian matrix equals a constant,  $n_Q = \sqrt{n_c} + 2$ . This coincides with the situation obtained by Belytschko et al. (1994). For the present three-dimensional structural analysis,  $D = 3$ , Eqn.(15) leads

$$n_Q \geq \sqrt[3]{n_c} + 3.$$

To perform the integration for evaluating the stiffness matrix  $K$  and load vector  $R$  of Eqn.(9), a set of three-dimensional cells as indicated by dashed lines in Fig.1 can be arranged. When the structure  $\Omega$  is split up into a number of cells  $\Omega_{ci}$ , with boundaries  $\Gamma_{ti}$  and  $\Gamma_{ui}$ , several regulations are held during the arranging process. The

geometric boundary and cell boundaries should be consistent each other. Each cell should include at least one node. It is noted that a null node cell will induce trivial integration.

Belytschko et al. (1994) presented an useful implementation procedure for the EFGM, which made the computation systematically and efficiently. This practical procedure is also generalized for the present three-dimensional structural analysis:

(a) Generate nodes and define basis functions  $p(x)$  and weighting functions  $w_i(x)$  such that the moving least squares approximation is well established.

(b) Determine cells for structure  $\Omega$  and boundaries  $\Gamma_u$ , and  $\Gamma_t$ . If a boundary segment exists in a cell or any linkage of quadrature points intersects the boundary segment, divide the cell or modify its shape.

(c) Choose Gaussian quadrature for each cell  $\Omega_{ci}$  by the relation of Eqn.(15).

(d) Compute nodal interpolation functions  $\phi_i(x)$  and its derivatives  $\phi_{i,j}(x)$  for those nodes in the cell. Evaluate and assemble the cell stiffness matrix and load vector to form Eqn.(9).

(e) Solve the linear system of Eqn.(9) for D.

As discussed above, although EFGM does not involve elements, but it does need cell structure to evaluate the stiffness matrix K and load vector R. By assembling the cell structure, Eqn.(4) can be rewritten as

$$\Pi = \sum_{i=1}^{N_c} \int_{\Omega_{ci}} (\frac{1}{2} \epsilon^T E \epsilon - u^T b) d\Omega_{ci} - \sum_{i=1}^L \int_{\Gamma_{ti}} u^T \bar{t}_i d\Gamma_{ti} = \min.$$

where  $N_c$  is the total number of cells and  $L$  is the divided number of traction boundaries.

Although the cells of EFGM are free to collocate in the structure after taking into account of the cell continuity, fewer nodes in a cell are usually suggested for computational efficiency. Besides, modifications for cells sometimes are required for geometric restrictions or computational efficiency improvement, especially for three-dimensional problems. By the same nodal collocation, some typical examples of modifications are demonstrated in Fig.5. No matter what kinds of modifications they are, null cell is not a clever arrangement.

### 5 Generation of Nodes

In finite element analysis, nodes are connected by elements, therefore, they are not able to add or delete freely.

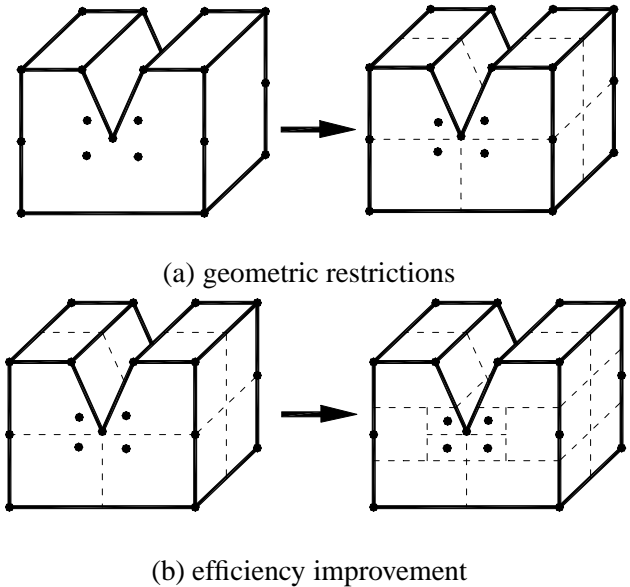


Figure 5 : Modifications of cells

In EFGM analysis, however, each node of the nodal set  $X = \{x_1, x_2, \dots, x_N\}$  is independent each other. Hence, to assure the uniqueness of the nodal displacements D, the mapping between the nodal set X and the nodal displacements D should be homeomorphic. That is, the nodal set X should be a metric space and satisfy the valuation theory in the valuation set (the nodal displacements D).

Let  $d(x_1, x_2)$  denote the distance from  $x_1$  to  $x_2$ . For a three-dimensional structure satisfying the compatibility condition, the nodal set X is a metric space if it satisfies the following conditions (Mendelson 1962):

- (a)  $d(x_1, x_2) \geq 0$  for all  $x_1, x_2 \in X$ ,
  - (b)  $d(x_1, x_2) = 0$  if and only if  $x_1 = x_2$ ,
  - (c)  $d(x_1, x_2) = d(x_2, x_1)$  for all  $x_1, x_2 \in X$ ,
- and
- (d)  $d(x_1, x_3) \leq d(x_1, x_2) + d(x_2, x_3)$  for all  $x_1, x_2, x_3 \in X$ .

Because the Euclidean coordinate system is adopted, all material points of the structure form a metric space and, therefore, the nodal set X should be a metric space. In addition, since each node has three components of nodal displacements which form the valuation set (the nodal displacements D), the nodal set X also satisfies valuation theory.

Consequently, the nodal displacements D exist and unique no matter how the nodal set X is divided for EFGM analysis. In this work, the nodal set X is divided

into three independent subsets. These three subsets come from three sequential steps for generating nodes in the solution procedure, say, defining the geometric boundary, arranging inside of the body, and improving numerical accuracy, if any. The nodal subsets corresponding to those three sequential steps are represented as  $X_{boundary}$ ,  $X_{body}$ , and  $X_{improvement}$ . The combined nodal set  $X$  is then found as

$$X = X_{boundary} + X_{body} + X_{improvement} \quad (16)$$

The nodal subset of numerical improvement  $X_{improvement}$  can be applied freely without destroying the linkages of the three-dimensional scattering sub-domains, except the sub-domain relating to the changed nodes.

## 6 Results and Discussions

To evaluate the validity and efficiency of the EFGM presented, three examples are examined. The first example is presented for demonstrating the merits of this work for three-dimensional structural analysis. The comparison of computational efficiency between the present EFGM and finite element method is also shown. The second example exhibits the flexibility of the present EFGM for analyzing a sphere subjected to a diametrical loading. The last example shows the superiority of the three-dimensional scattering sub-domain devised in this work. All structures are manufactured by steel with Young's modulus  $E=200 \text{ GPa}$  and Poisson ratio  $\nu = 0.3$ .

A short beam containing a circular cylinder subjected to uniform loading at both ends as shown in Fig.6 is first analyzed. The finite element models using 8-node brick elements and 20-node quadratic elements as seen in Fig.7 (a) and (b) are carried out. The computed stress concentration factors  $K_{\sigma}$  near the positions A and B are listed in Table1 and compared with those quoted by Peterson (1974). For comparison purposes, the same nodal collocations as the linear and quadratic element discretizations are also adopted for the present EFGM computation. As seen from Table1, it is obvious that the present EFGM is much more accurate but with a little expensive CPU times. In fact, such nodal collocations can not demonstrate the advantages of the present EFGM in dealing with three-dimensional structural problem. An alternative nodal collocation with 198 nodes (much less) as

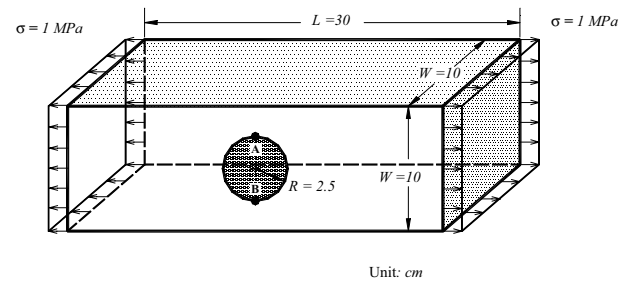


**Figure 6 :** Three-dimensional stress concentration analysis

displayed in Fig.8 (a) is generated by the two steps of defining the geometric boundary and arranging inside of the body. To Further improve the accuracy of the stress concentration factors  $K_{\sigma}$ , the third step of improving numerical accuracy is made by adding nodes near A and B (see Fig.8 (b)). Excellent efficiency with difference 0.93% and 54 CPU sec. is achieved.

A sphere under a diametrical loading at two poles as seen in Fig.9 is then solved. Also shown in Fig.9 is the nodal collocation at various sections of the sphere with 63 nodes. Although finite element method has been widely used, sometimes, the geometric boundary can not be treated whenever a specific properly element type is used. To deal with the problem like this example, much refined mesh as accompanies by ill shape elements is often employed. This example also presents the flexibility of the EFGM developed in solving three-dimensional structural problems. Fig.10 displays the constant von Mises stress contours on the surface of the sphere. Also shown for comparison purposes is the analytical solution on the spherical surface based on the theory of elasticity (Timoshenko et al., 1970), which is derived as

$$\begin{aligned} \sigma_z &= -\frac{P}{8\pi(1-\nu)} \left[ \frac{(1-2\nu)(R^2-3z^2)}{R^4} + \frac{3z^2(3R^2-5z^2)}{R^6} \right], \\ \sigma_r &= \frac{P}{8\pi(1-\nu)} \left[ \frac{(1-2\nu)(R^2-3z^2)}{R^4} - \frac{3(R^2-z^2)(R^2-5z^2)}{R^6} \right], \\ \sigma_{\theta} &= \frac{P(1-2\nu)(R^2-3z^2)}{8\pi R^4(1-\nu)}, \\ \tau_{rz} &= -\frac{P}{8\pi(1-\nu)} \left[ \frac{3z(1+2\nu)\sqrt{(R^2-z^2)}}{R^4} - \frac{15z^3\sqrt{(R^2-z^2)}}{R^6} \right], \end{aligned}$$

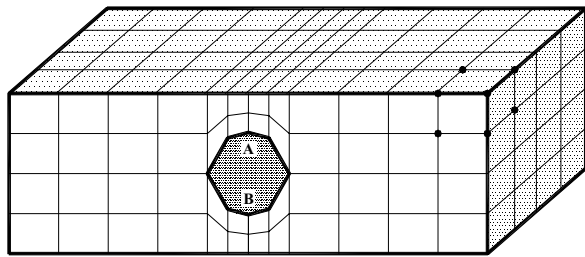
and

$$\tau_{r\theta} = \tau_{\theta z} = 0.$$

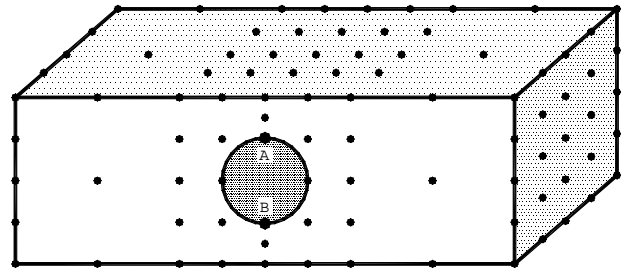
More accurate results in the neighborhood of two loading

**Table 1** : The comparisons for FEM and EFGM

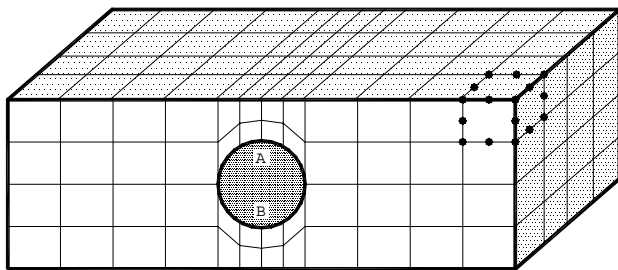
		Cells	Elements	nodes	$K_{\sigma}$	differences	CPU(sec)
Peterson (1974)		-	-	-	2.16	-	-
FEM	I(8 nodes)	-	192	325	1.76	18.51%	181
	II(20 nodes)	-	192	1,145	2.06	4.63%	428
EFGM	I	325	-	325	2.02	6.48%	292
	II	1,145	-	1,145	2.14	0.93%	1,421
	Original	198	-	198	1.98	8.33%	32
	Modified	218	-	218	2.14	0.93%	54



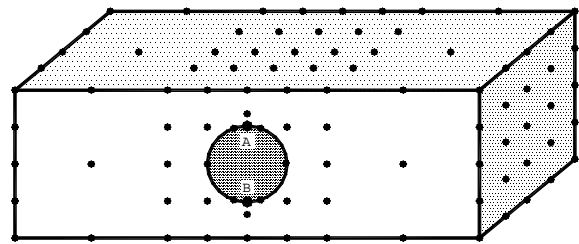
elements: 192  
nodes: 325  
(a) 8-node brick element



nodes: 198  
(a) original



elements: 192  
nodes: 1,145  
(b) 20-node quadratic element



nodes: 218  
(b) modified

**Figure 8** : Different node collocations for the EFGM

**Figure 7** : Finite element discretizations for stress concentration problem

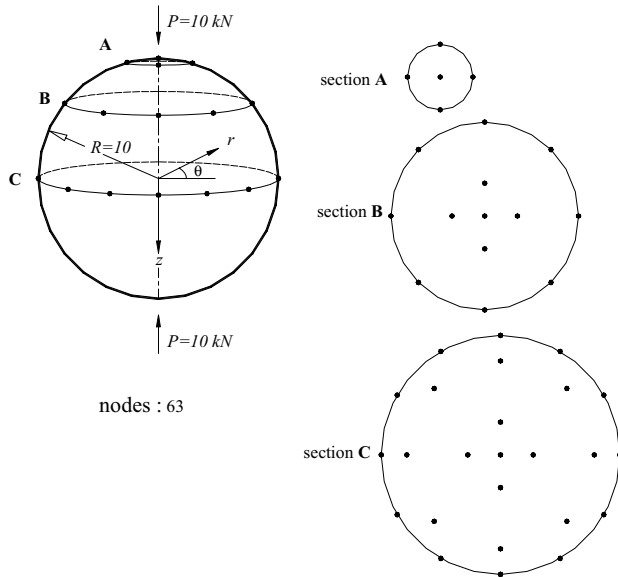


**Figure 9 :** A sphere under a diametrical loading at two poles

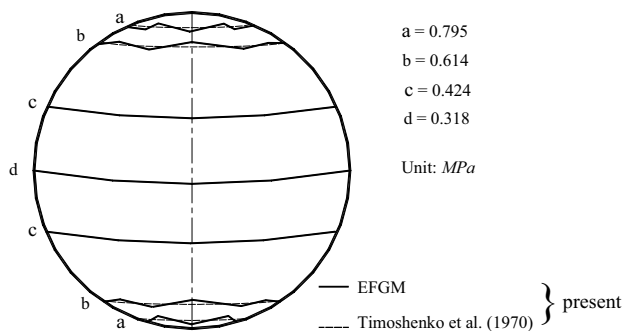


**Figure 10 :** The von Mises stress contours on the spherical surface

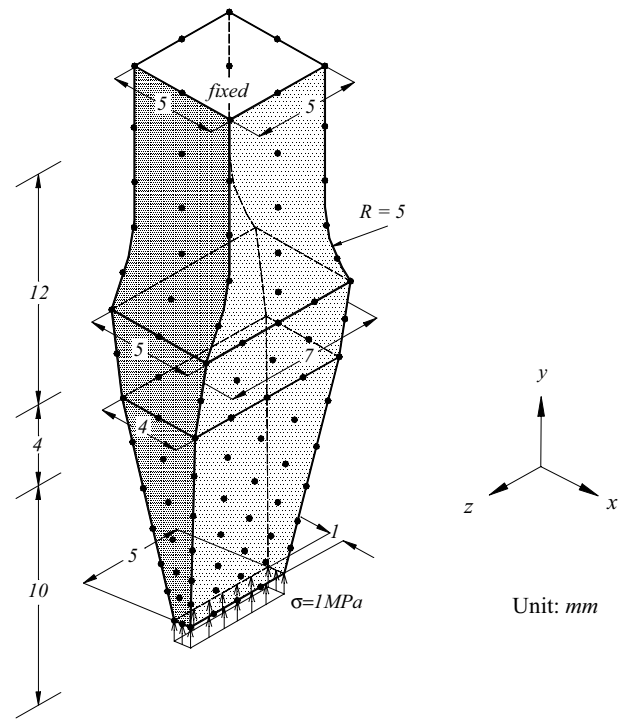


**Figure 11 :** The forward motion of a screwdriver

poles can be achieved by further modified node generation.

To demonstrate the novelty of the three-dimensional scattering sub-domain devised in executing moving least squares approximation among nodes with different densities, the forward motion of a screwdriver as described in Fig.11 is finally analyzed. Since the bottom end needs more nodes to achieve finer stress resolution, the nodal generation differs from other positions. The three-dimensional scattering sub-domain fully exhibits its superiority by the changeable size of linkages. The computed results and those calculated by the mechanics of strength of materials are drawn in Fig.12. The latter approximated solution can be written as

$$\sigma_y = \frac{5}{A}, \tag{17}$$

where  $A$  is the area of various cross sections of the screwdriver paralleling to  $x - z$  plane. These differences perhaps are caused by the stress concentration around corners, which can not be accounted for by Eqn.(17). By this example, the present EFGM shows its advantages and

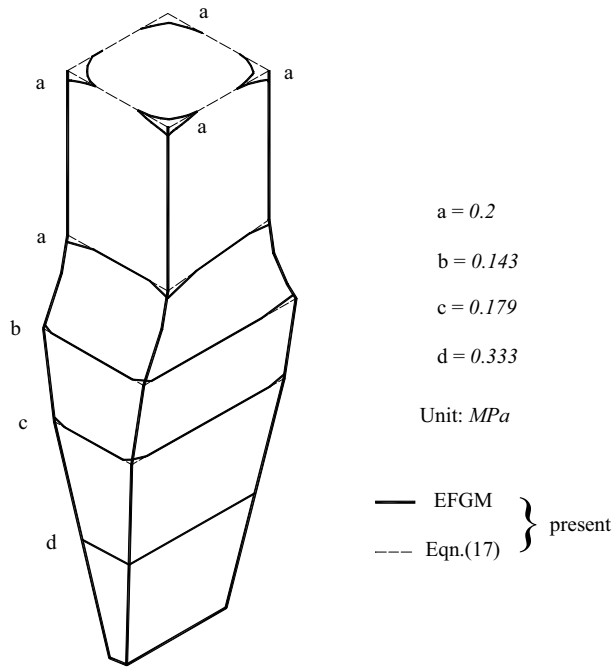


Figure 12 : von Mises stress contours of a screwdriver

flexibility in changing the size of linkages and number of nodes in the three-dimensional scattering sub-domains.

### 7 Conclusions and Recommendations

An accurate and efficient EFGM has been successfully established to deal with three-dimensional structural problems. The three-dimensional scattering sub-domain with changeable size of linkages demonstrates its superiority in minimizing the bandwidth of stiffness matrix but maintaining the accuracy. The relation between the quadrature orders  $n_Q$  and the number of nodes in a cell  $n_c$  is rigorously examined. The flexibility of generating nodes for the present three-dimensional structural analysis is also developed. The present EFGM technique can be further extended to analyze other three-dimensional structural problems, for examples, the problems with geometric/material nonlinear behaviors, etc.

### Appendix A. The nodal interpolation functions

$$\phi_i(\xi, \eta, \zeta)$$

In this work, a cubic cell with a node  $i$  at its center is considered. After mapping from global coordinates  $\{x, y, z\}$  to natural coordinates  $\{\xi, \eta, \zeta; -1 \leq \xi, \eta, \zeta \leq 1\}$ , one has

$$\begin{aligned} \phi_i(x) &= \phi_i(\xi, \eta, \zeta) = \sum_{k=1}^K c_k \xi^r \eta^s \zeta^t \\ &= (1 - \xi^2) (1 - \eta^2) (1 - \zeta^2) \\ &= 1 - \xi^2 - \eta^2 - \zeta^2 + \xi^2 \eta^2 + \eta^2 \zeta^2 + \zeta^2 \xi^2 - \xi^2 \eta^2 \zeta^2, \end{aligned}$$

where the number of terms  $K$  equals 8. The order of nodal interpolation function  $\phi_i(\xi, \eta, \zeta)$  is

$$r + s + t = 6 \geq m + D = 4. \quad (m = 1; D = 3)$$

The quadrature orders  $n_Q$  is therefore determined by

$$n_Q \geq \sqrt[3]{n_c} + D = 4. \quad (n_c = 1)$$

As mentioned above, since each cell used in this work is always with a node at its center, hence, the quadrature orders  $n_Q$  is taken as 4 for all calculations. As curved surface becomes part of the cell, higher quadrature orders  $n_Q$  is a better choice for such cell.

### References

- Atluri, S. N.; Zhu, T. (1998a): A new Meshless Local Petrov-Galerkin (MLPG) approach in computational mechanics. *Comput. Mech.*, Vol.22, pp.117-127.
- Atluri, S. N.; Kim, H. G.; Cho, J. Y. (1999): A critical assessment of the truly Meshless Local Petrov-Galerkin (MLPG) and Local Boundary Integral Equation (LBIE) methods. *Comput. Mech.*, 24: (5), pp.348-372.
- Atluri, S. N.; Sladek, J.; Sladek, V. (2000a): The Local boundary Integral Equation (LBIE) and it's meshless implementation for linear elasticity. *Comput. Mech.*, 25:(2-3), pp.180-198.
- Atluri, S. N.; Zhu, T. L. (2000b): The Meshless Local Petrov-Galerkin (MLPG) approach for solving problems in elasto-statics. *Comput. Mech.*, 25(2-3), pp.169-179.
- Belytschko, T.; Lu, Y. Y.; Gu, L. (1994): Element Free Galerkin Methods. *Int. J. Numer. Methods Eng.*, Vol.37, pp.229-256.
- Belytschko, T.; Organ, D.; Krongauz, Y. (1995): A coupled finite element – Element Free Galerkin Method. *Comput. Mech.*, Vol.17, pp.186-195.
- Belytschko, T.; Krysl, P. (1996a): Analysis of thin shells by the Element Free Galerkin Method. *Int. J. Solids Structures.*, Vol.33, pp.3057-3080.

- Belytschko, T.; Krongauz, Y.** (1996b): Enforcement of essential boundary conditions in meshless approximations using finite element. *Comput. Methods Appl. Mech. Eng.*, Vol.131, pp.133-145.
- Belytschko, T.; Krongauz, Y.; Fleming, M.; Organ, D.; Liu, W. K. S.** (1996c): Smoothing and accelerated computations in the Element Free Galerkin Method. *Comput. Methods Appl. Mech. Eng.*, Vol.74, pp.111-126.
- Belytschko, T.; Krysl, P.** (1997): Element Free Galerkin Method convergence of the continuous and discontinuous shape function. *Comput. Methods Appl. Mech. Eng.*, Vol.148, pp.257-277.
- Ching, H.K.; Batra, R.C.** (2001): Determination of Crack-tip Fields by the Meshless Local Petrov-Galerkin (MLPG) Method, *CMES: Computer Modeling in Engineering & Sciences*, Vol.2, No.2, pp273-290.
- Chinn, W. G.; Steenrod, N. E.** (1966): *First Concepts of Topology/ The Geometry of Mappings of Segments, Curves, Circles, Disks, and Spheres*. Random House, New York.
- Cook, R. D.; David, S. M.; Michael, E. P.** (1989): *Concepts and Applications of Finite Element Analysis*. John Wiley and Sons, Inc.
- Hegen, D.** (1996): Element Free Galerkin Methods in combination with finite element approaches. *Comput. Methods Appl. Mech. Eng.*, Vol.135, pp.143-166.
- Kim, H.G.; Atluri, S. N.** (2000c): Arbitrary placement of secondary nodes, and error control, in the Meshless Local Petrov-Galerkin (MLPG) Method. *CMES: Computer Modeling in Engineering & Sciences.*, Vol.1: (3), pp.11-32.
- Lin, H.; Atluri, S. N.** (2000d): Meshless Local Petrov-Galerkin (MLPG) Method for convection-diffusion problems. *CMES: Computer Modeling in Engineering & Sciences.*, Vol.1: (2), pp.45-60.
- Lin, H.; Atluri, S. N.** (2001): The Meshless Local Petrov-Galerkin (MLPG) Method for solving incompressible Navier-stokes equations. *CMES: Computer Modeling in Engineering & Sciences.*, Vol.2: (2), pp.117-142.
- Mendelson, B.** (1962): *Introduction to topology*. Allyn and Bacon, Boston.
- Mukherjee, Y. X.; Mukherjee, S.** (1997): On boundary conditions in the Element Free Galerkin Method. *Comput. Mech.*, Vol.18, pp.264-270.
- Nayroles, B.; Touzot, G.; Villon, P.** (1992): Generalizing the finite element method: diffuse approximation and diffuse elements. *Comput. Mech.*, Vol.10, pp.307-318.
- Peterson, R. E.** (1974): *Stress concentration factor*. John Wiley and Sons, Inc.
- Stroud, A. H.; Secrest, D.** (1966): *Gaussian Quadrature Formulas*. Englewood Cliffs, N.J., Prentice-Hall.
- Timoskenko S. P.; Goodier J. N.** (1970): *Theory of Elasticity*. 3<sup>rd</sup> Edn, McGraw-Hill, New York.
- Zhu, T.; Atluri, S. N.** (1998b): A modified collocation method and a penalty formulation for enforcing the essential boundary conditions in the Element Free Galerkin Method. *Comput. Mech.*, Vol.21, pp.211-222.
- Zhu, T.; Zhang, J.; Atluri, S. N.** (1998c): A Meshless Local Boundary Integral Equation (LBIE) method for solving nonlinear problems. *Comput. Mech.*, Vol.22: (2), pp.174-176.